Vacuum 153 (2018) 112–116

Contents lists available at ScienceDirect

Vacuum

journal homepage: www.elsevier.com/locate/vacuum

# An investigation on the half-cell production for transparent secondary type solid-state batteries

Soner Özen [a, *], Suat Pat [a], H. Hakan Yudar [a], Şadan Korkmaz [a], Zerrin Pat [b]

[a] Eskişehir Osmangazi University, Physics Department, 26480, Eskişehir, Turkey
[b] Bilecik Şeyh Edebali University, Chemistry Department, Bilecik, Turkey

ARTICLE INFO

*Article history:*
Received 2 November 2017
Received in revised form
19 February 2018
Accepted 22 March 2018
Available online 5 April 2018

*Keywords:*
LCO
LPO
Solid-state battery
Transparent battery
Morphological properties
Impedance analysis

ABSTRACT

In this research, the effects on battery characteristics of two different production methods were investigated. The $Li_3PO_4/LiCoO_2$/ITO/glass half-cell designs have been produced and analyzed. The $LiCoO_2$ cathode layers are deposited on the ITO/glass substrates by using radio frequency magnetron sputtering method. The $Li_3PO_4$ electrolyte layers are coated on this structure by using radio frequency magnetron sputtering and thermionic vacuum arc afterward. The optical, morphological, and electrochemical properties of the produced half-cells are investigated by various analyzed methods. It is seen that the produced half-cells have high transmittance values and relevant optical band gap values. When the radio frequency power is increased from 100 W to 125 W, more rough structures are formed. The cell1 produced by the thermionic vacuum arc method has exhibited more porous structure in the production of the electrolyte layer. This conjuncture clearly influenced the ionic conductivity.

© 2018 Elsevier Ltd. All rights reserved.

The secondary lithium batteries are lately utilized as a power supply for electronic and hybrid electronic devices as well as disquiet about the lack of energy sources and environmental pollution [1–6]. There is a growing interest in the production of secondary lithium batteries of smaller dimensions. The layers of secondary type battery materials such as cathode layer, an electrolyte layer, anode layer are low optical transmittance except for the electrolyte layer [7–10]. The solid transparent electrolyte which has a high ionic conductivity is more important material for the secondary type battery performance [11–13]. The solid-state electrolyte layer is permeable to lithium ions and it is impermeable as electronic insulator [14–17]. The $Li_3PO_4$ (LPO) is an alternative electrolyte for fully transparent solid-state batteries [12,18–21]. LiCoO2 (LCO) is widely used as a cathode in commercialized secondary lithium batteries [6,22–24]. The d-d transitions underwent a blue shift of about 0.3 eV as the cubic LCO transformed into the rhombohedral structure with band gap values of about 1.4 and 1.7 eV [25]. A band gap of 2.4 eV has been found by Ensling et al. [26]. In the modified-spinel (disordered-phase) films, only a prominent peak was observed at 2.9 eV, while the shoulder disappeared [27]. a linear extrapolation of the energy axis gave a bandgap energy of 2.5 eV [28]. The $Li_xCo_{1-x}O$ which has a larger gap (2.7 eV) than CoO was closed the band gap value with increasing x to 2.0 eV for $x = 0.2$ [29].

The Li ion battery layers can be produced by means of various techniques. These techniques can be given as RF sputtering [7,9,26], chemical vapor deposition [2,30–32], pulsed laser deposition [1,33,34], DC sputtering [22], combustion process [24,25], solvothermal reaction [28,29], sol-gel method [6,35], spin-coating technique [8], solvent casting method [13], molten salt method [23], thermal evaporation [36].

The transparent solid state half-cell productions are performed by using RF magnetron sputtering method (RF-MS) and thermionic vacuum arc method (TVA) and their half-cell designs and photography is presented in Fig. 1. RF-MS method is used for the cathode layer productions. It is used two different methods for the electrolyte layer production: TVA method for cell1 and RF-MS method for cell2. We used indium tin oxide (ITO) coated microscope slides as substrate.

RF-MS is a widely used thin film deposition technique. Low pressures of noble gas atoms on the order of $10^{-2}$-$10^{-3}$ Torr are fed into the chamber. The noble gas atoms are ionized as a result of collisions with electrons. The ions are not while the electrons are significantly influenced by the magnetic field. When they hit the target material, they remove atoms from the target as a result of

* Corresponding author.
*E-mail address:* sonerozen55@yahoo.co.uk (S. Özen).

https://doi.org/10.1016/j.vacuum.2018.03.041
0042-207X/© 2018 Elsevier Ltd. All rights reserved.

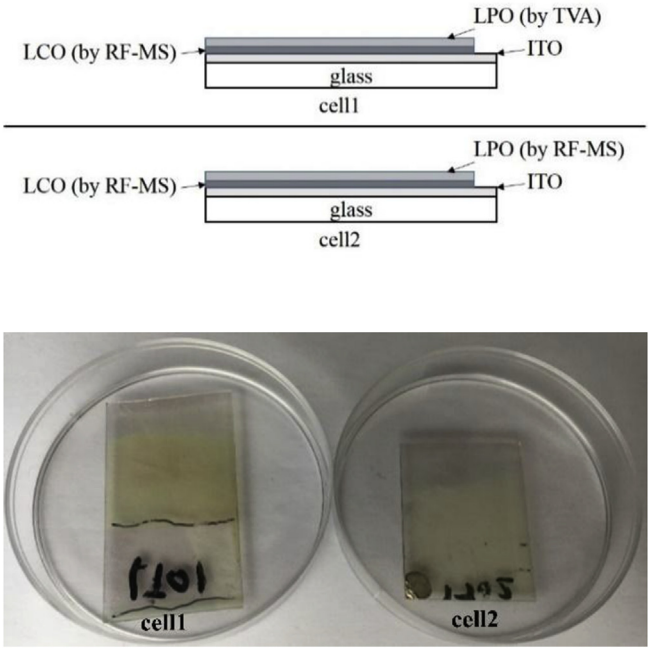


**Fig. 1.** The design and photography of the transparent cells produced by two different methods.

momentum transfer from large ions to target material. Sputtered target atoms are free of charge, so they are not affected by magnetic or electric field and can move towards the substrate and begin to form desired films. In RF-MS experiments, we used $Li_3PO_4$ target (purity: 99.9%) and $LiCoO_2$ target (purity: 99.9%) with a thickness of 0.125 inches and diameter of 2 inches as sputtering material. Pure argon gas was used as a buffer gas and was introduced through a needle valve. During the deposition, the sputtering was conducted in an Ar atmosphere with a target-to-substrate distance of 4 cm. The deposition chamber was initially pumped down to $2 \times 10^{-2}$ Torr for all experiments. For cathode layer deposition experiments, applied radio frequency (RF) powers were chosen as 100 W for cell1 and 125 W for cell2, working pressures were $6 \times 10^{-2}$ Torr, and deposition times were 45 min. For electrolyte layer of cell2, applied radio frequency (RF) power was chosen as 75 W, working pressure was $1 \times 10^{-1}$ Torr. The deposition time for all RF-MS experiments was 60 min.

The TVA discharge occurs between the anode and the cathode electrodes under high vacuum conditions. The anode electrode consists of the crucible and deposited material. The cathode filament which made from a tungsten wire with a diameter of 1 mm is mounted inside an electron-focusing Wehnelt cylinder. The accelerated electrons collide with the anode due to a high dc potential difference applied between the anode and cathode. The heated anode material melts firstly and after some time starts to boil and evaporate. With the increase of applied high voltage, a bright discharge occurs in the interelectrode space. The plasma ions are accelerated toward the vacuum vessel wall since the cathode of TVA is at earth potential. Thus the material to be coated starts to be deposited on the substrates. For electrolyte layer of cell1, the working pressure inside the vacuum vessel was about $1 \times 10^{-4}$ Torr, and the intensity of the heating current of the cathode filament was $I_f = 18$ A. The voltage applied to the space between anode and cathode was 250 V. The voltage dropped to 100 V and the current of the discharge was $I_d = 0.2$ A. The deposition process was carried out for 0.5 min.

The colors of produced half-cells were coded with the tricolor red-green-blue (RGB) color values. LCO films are lithium deficient when observation of the dark amber color [37]. It has the undesirable property. The color of the film shifts to blue as the Li ratio in the LCO film increases [35,38]. The RGB code of the dark amber color is (230, 120, 45). The RGB values from the cell1 and cell2 photos given in Fig. 1 are determined as (135, 120, 90) and (115, 110, 90), respectively. It is clear that the blue color code showed a higher value while the red color code shows a lower value.

The optical transmittances of the produced thin films were recorded at normal incidence of light with a UNICO 4802 UV–VIS double beam spectrophotometer. The optical transmittance in the wavelength range of 325–1000 nm, and Tauc plot for the produced thin films are shown in Fig. 2. The T(λ) curves of LCO/ITO coated glass, LPO/LCO/ITO coated glass, and the ITO coated glass substrate are also shown in the same figure for comparison. It is seen from the figure that the ITO coated glass substrate has a high transmittance value of 85–90% in the visible region. After LCO thin films were deposited on ITO coated glass substrate, the transmittances of samples decreased by about 10–20% in the visible region. The transmittances of samples decreased by 5% in the near infrared region. At the same time, the percent transmittance T% of the cell1 in the visible region is between 57% and 83% which is a little bit lower than that of the cell2 due to the increase in RF power. The

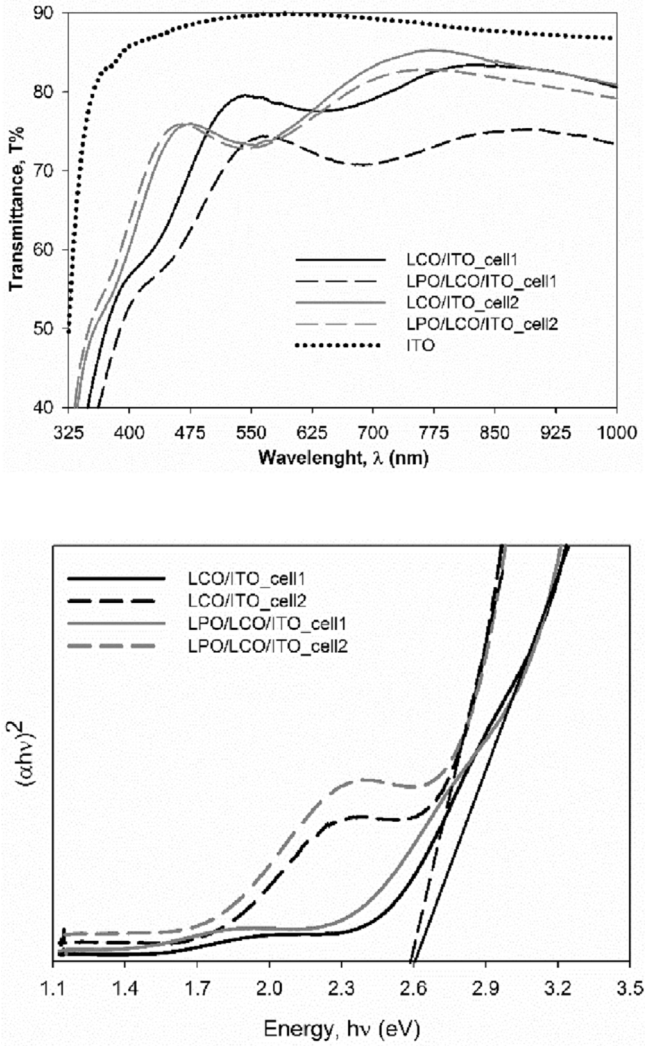


**Fig. 2.** The transmittance and optical band gap plots of the produced transparent solid-state cells.

transparency of the cell2 has decreased almost negligible together with the coating of the LPO layer by using RF-MS. However, the transmittance of the cell1 decreased by about 4–8% together with the coating of the LPO layer by using TVA. It can be said that more porous layer occurs by using TVA method. The optical band gaps of the produced cells were evaluated from their UV-VIS absorbance spectra. By extrapolating the linear part of the Tauc plot $(\alpha h\nu)^2$ vs. $h\nu$ on the energy axis gives the optical band gap value. The band gap value of 2.6 eV is associated with LCO thin film [27–29]. Since the band gap value of the LPO material is below the band edge of the glass, it cannot be observed [12]. According to Tauc plot of cell2, second energy value in the band gap value of 1.7 eV is associated with cubic LCO transformed into the rhombohedral structure [25].

The surface morphology, surface roughness, and height distribution histogram were determined by using an Ambios Q-Scope atomic force microscope (AFM) with the ScanAtomic V5.1.0 SPM control software in non-contact mode. The 3D AFM images and results of the histogram analysis such as average height ($h_a$), average surface roughness ($r_{rms}$), maximum deviation ($\sigma_{max}$), skewness ($S_{sk}$), kurtosis ($S_{kr}$) are presented in Fig. 3. The images of LCO thin films showed a dense and granular film structure with spherical grains of varying sizes. But, the surface images of half-cells showed flat and wavy film structure after LPO layer production. The LPO layers were spread like nappe onto the surface. A

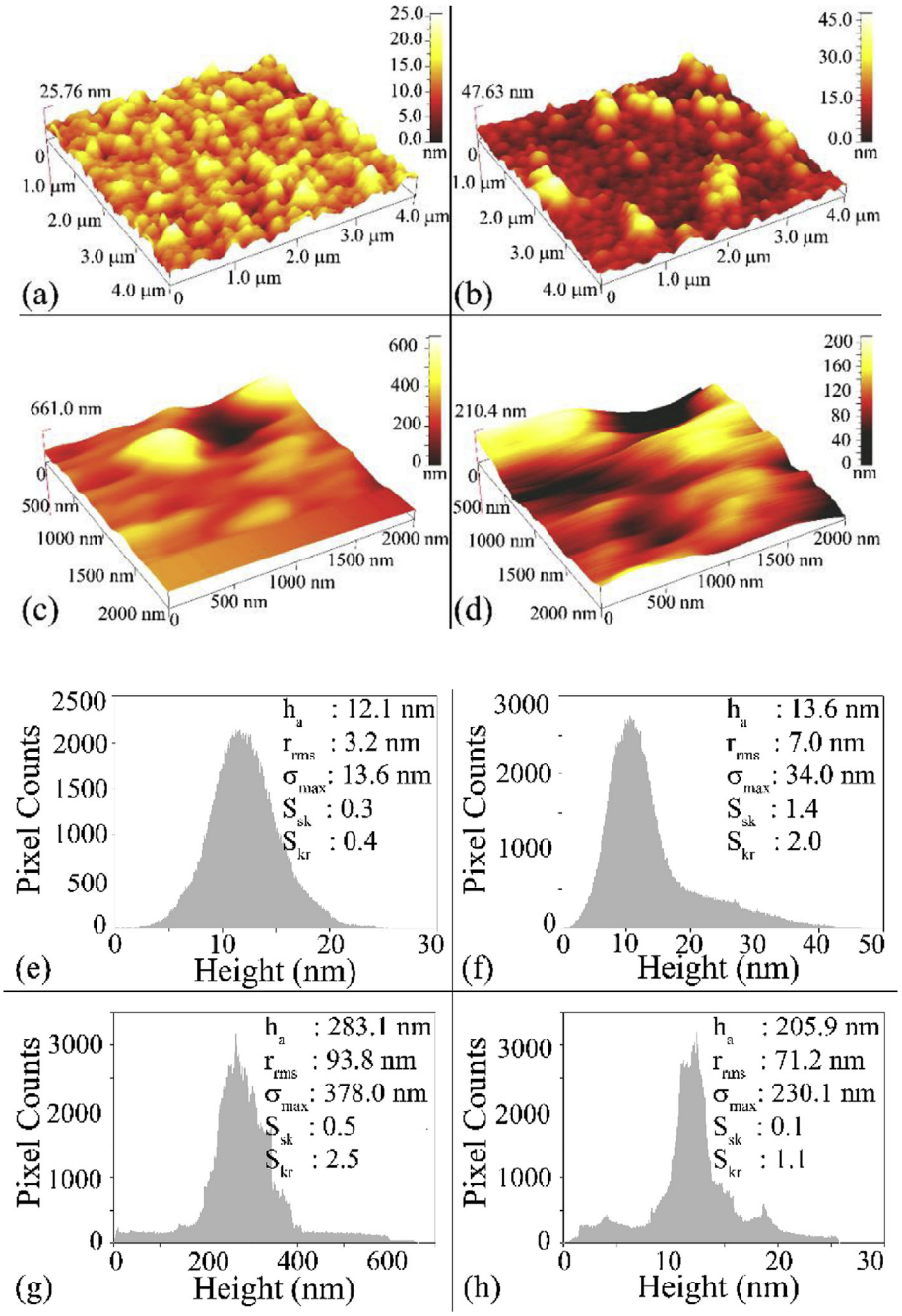


**Fig. 3.** The 3D AFM image of (a) the $LiCoO_2$ layer for cell 1, (b) the $LiCoO_2$ layer for cell 2, (c) the $Li_3PO_4/LiCoO_2$ layer for cell 1, (d) the $Li_3PO_4/LiCoO_2$ layer for cell 2 on ITO coated glass substrate, the histogram analysis of (e) the $LiCoO_2$ layer for cell 1, (f) the $LiCoO_2$ layer for cell 2, (g) the $Li_3PO_4/LiCoO_2$ layer for cell 1, and (h) the $Li_3PO_4/LiCoO_2$ layer for cell 2 on ITO coated glass substrate.

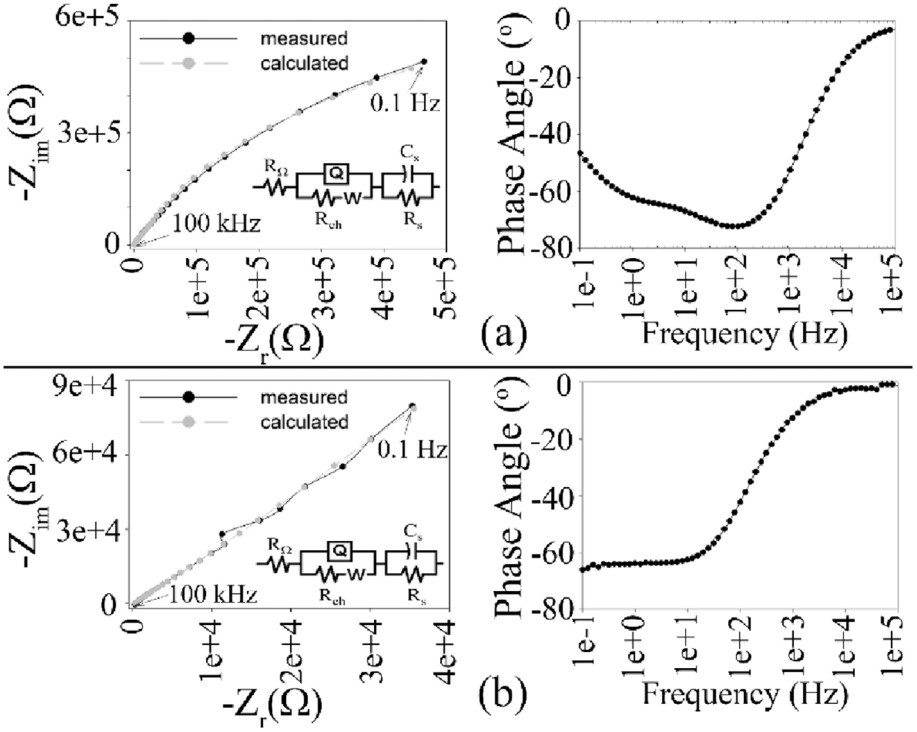


**Fig. 4.** Complex plane plot of the impedance and phase angle as a function of frequency for (a) the cell1, (b) cell2.

perfect symmetrical surface distribution has a skewness value equal to zero. If the surface distribution has more peaks than valleys the skewness value will be positive. Kurtosis value is a measure of the flatness of the distribution. The normal surface distribution has a kurtosis value equal to zero. If the kurtosis value is positive surface topography will imply a sharply peaked distribution. While the surface of the cell is an asymmetric rough structure in the deposition process by using TVA method, the surface of the cell is a symmetric flat-topped structure in the deposition process by using RF-MS method.

For electrochemical measurements of the lithium-ion cells, we used ITO as the counter electrode, Ag as a reference electrode, half-cells as the working electrode, and the electrolyte was a 1 M LiClO4 solution in propylene carbonate (PC). The conductivity of the electrolyte was approximately 2.0 mS/cm. A potentiostat/galvanostat/ZRA (Gamry Reference 3000 instrument) was used for the electrochemical measurements. Electrochemical impedance spectroscopy was carried by applying an AC voltage of 0.5 V in a frequency range of 0.1 Hz−100 kHz at an open circuit potential.

The impedance spectra of the cells are fitted according to the equivalent circuit which a modification of the well-known Randles circuit and the fitted results are shown in Fig. 4. In the equivalent circuits, Q which constant-phase element consists of two parameters. These two parameters are $Y_0$ which frequency independent constant and n which correction factor. $R_\Omega$ represents the contact resistance between electrolyte and electrodes. $R_{ch}$ is the charge transfer resistance, and W is the Warburg impedance. $R_s$ is the separator resistance, and $C_s$ is the separator capacitance. The Li diffusivity is low when the thickness of the cathode electrode is thin. There is the effect on diffusion of the $Li^+$ in the cathode material of the cathode and cathode-electrolyte interface. Increase in porosity and roughness increase ionic conductivity [39,40]. Impedance phase angles exhibit a closed 90° slope at which is characteristic of a pronounced capacitive behavior. The 45° phase angle was present at 1504 Hz for cell1, at 83 Hz for cell2, demonstrating the fast accessibility of the ions in cell1. The decrease at 100 Hz after the increase of the phase angle at low frequencies shows that the cathode-electrolyte interface is porous [36]. The conjectural results of each circuit component of produced half-cells are listed in Table 1. Q becomes a pure capacitor when the correction factor is 1. If correction factor is 0.5, Q becomes a Warburg impedance. The chi-squared ($\chi^2$) values are $3.8 \times 10^{-4}$ for cell1 and $2.3 \times 10^{-4}$ for cell2. The low W values of the cells showed us that the Li-ion diffusion is easier, but the charge transfer of cells is low due to high resistance, especially cell1. The cell1 showed capacitance value of 1.9 μF while the cell2 showed capacitance value of 51 μF.

The effects on battery characteristics of experimental parameters for the LPO/LCO/ITO/glass half-cells were investigated. No thermal treatment has been applied after the thin film layer deposition processes for half-cell production. The RGB codes of produced half-cells are observed as (135, 120, 90) for cell1 and (115, 110, 90) for cell2. The red dominant color code in the dark amber color is weaker for cell2 according to cell1. In this point, we reached the conclusion that the Li ratio in the cathode layer of the cell2 produced by using RF-MS is higher than the Li ratio in the cathode

**Table 1**
The equivalent circuit element values of produced half-cells.

| | $R_\Omega$ (Ω.cm$^2$) | $Y_0$ (S.sec$^n$.cm$^{-2}$) | n | $R_{ch}$ (Ω.cm$^2$) | W (S.sec$^{0.5}$.cm$^{-2}$) | $C_s$ (F.cm$^{-2}$) | $R_s$ (Ω.cm$^2$) |
|---|---|---|---|---|---|---|---|
| cell1 | 289 | $2 \times 10^{-6}$ | 0.82 | $0.9 \times 10^6$ | $32 \times 10^{-9}$ | $2 \times 10^{-6}$ | $8 \times 10^3$ |
| cell2 | 378 | $14 \times 10E^{-6}$ | 0.76 | $0.3 \times 10^6$ | $1 \times 10^{-6}$ | $51 \times 10^{-6}$ | $1 \times 10^3$ |

layer of the cell 1 due to the influence of RF power. The high transparency cells were produced by both production methods. A dense and granular film structure with spherical grains of varying sizes was detected from the AFM analysis of LCO thin films. The cell2 sample showed a more porous structure with the influence of RF power. However, the AFM images of half-cells presented a flat structure spread like nappe onto the surface after LPO layer productions. The porous structures were better obtained by TVA technique. The electrochemical analysis results showed that the Li-ion diffusion is easier in the cell1 half-cell than cell2, while the charge transfer of half-cells is low for cell1. It was concluded that it is better to increase RF power in RF-MS method for cathode layer production and TVA method is quite suitable for porous structures. It is possible to obtain more smooth surfaces by modifying TVA parameters.

## Acknowledgement

This work was supported by The Scientific and Technological Research Council of Turkey (Grant Number is 115E331).

## Appendix A. Supplementary data

Supplementary data related to this article can be found at https://doi.org/10.1016/j.vacuum.2018.03.041.

## References

[1] I. Yamada, K. Miyazaki, T. Fukutsuka, Y. Iriyama, T. Abe, Z. Ogumi, Lithium-ion transfer at the interfaces between LiCoO 2 and LiMn 2 O 4 thin film electrodes and organic electrolytes, J. Power Sources 294 (2015) 460–464.
[2] G.P. Pandey, S.A. Klankowski, T. Liu, J. Wu, J. Li, Toward highly stable solid-state unconventional thin-film battery-supercapacitor hybrid devices: interfacing vertical core-shell array electrodes with a gel polymer electrolyte, J. Power Sources 342 (2017) 1006–1016.
[3] Z.S. Wu, K. Parvez, X. Feng, K. Müllen, Graphene-based in-plane micro-supercapacitors with high power and energy densities, Nat. Commun. 4 (2013).
[4] R. Li, Y. Wang, C. Zhou, C. Wang, X. Ba, Y. Li, X. Huang, J. Liu, Carbon-stabilized high-capacity ferroferric oxide nanorod array for flexible solid-state alkaline battery–supercapacitor hybrid device with high environmental suitability, Adv. Funct. Mater. 25 (33) (2015) 5384–5394.
[5] W. Wang, N. Wang, A. Vinco, R. Siddique, M. Hayes, B. O'Flynn, C. O'Mathuna, Super-capacitor and Thin Film Battery Hybrid Energy Storage for Energy Harvesting Applications, IOP Publishing, 2013, p. 012105. Journal of Physics: Conference Series.
[6] X. Wang, Q. Qu, Y. Hou, F. Wang, Y. Wu, An aqueous rechargeable lithium battery of high energy density based on coated Li metal and LiCoO 2, Chem. Commun. 49 (55) (2013) 6179–6181.
[7] S. Özen, V. Şenay, S. Pat, Ş. Korkmaz, Optical, morphological properties and surface energy of the transparent Li4Ti5O12 (LTO) thin film as anode material for secondary type batteries, J. Phys. Appl. Phys. 49 (10) (2016) 105303.
[8] F. Martín, E. Navarrete, J. Morales, C. Roldán, J.R. Ramos-Barrado, L. Sánchez, High-energy, efficient and transparent electrode for lithium batteries, J. Mater. Chem. 20 (14) (2010) 2847–2852.
[9] H. Lee, H. Yim, K.-B. Kim, J.-W. Choi, Optical properties and electrochemical performance of LiFePO4 thin films deposited on transparent current collectors, J. Nanosci. Nanotechnol. 15 (11) (2015) 8627–8631.
[10] A.B. Béléké, C. Faure, M. Röder, P. Hovington, U. Posset, A. Guerfi, K. Zaghib, Chemically fabricated LiFePO 4 thin film electrode for transparent batteries and electrochromic devices, Mater. Sci. Eng., B 214 (2016) 81–86.
[11] D.F. Miranda, C. Versek, M.T. Tuominen, T.P. Russell, J.J. Watkins, Cross-linked block copolymer/ionic liquid self-assembled blends for polymer gel electrolytes with high ionic conductivity and mechanical strength, Macromolecules 46 (23) (2013) 9313–9323.
[12] S. Pat, S. Özen, V. Şenay, Ş. Korkmaz, Optical and surface properties of optically transparent Li3PO4 solid electrolyte layer for transparent solid batteries, Scanning 38 (4) (2016) 317–321.
[13] R. Leones, R.C. Sabadini, J.M. Esperança, A. Pawlicka, M.M. Silva, Effect of storage time on the ionic conductivity of chitosan-solid polymer electrolytes incorporating cyano-based ionic liquids, Electrochim. Acta 232 (2017) 22–29.
[14] L. Fei, Y. Xu, X. Wu, Y. Li, P. Xie, S. Deng, S. Smirnov, H. Luo, SBA-15 confined synthesis of TiNb 2 O 7 nanoparticles for lithium-ion batteries, Nanoscale 5 (22) (2013) 11102–11107.
[15] E. Peled, F. Patolsky, D. Golodnitsky, K. Freedman, G. Davidi, D. Schneier, Tissue-like silicon nanowires-based three-dimensional anodes for high-capacity lithium ion batteries, Nano Letters 15 (6) (2015) 3907–3916.
[16] L. Zhong, L. Mangolini, Nanomaterials in anodes for lithium ion batteries: science and manufacturability, Nanosci. Nanotechnol. - asia 5 (2) (2015) 68–89.
[17] C.B. Bucur, A. Lita, N. Osada, J. Muldoon, A soft, multilayered lithium–electrolyte interface, Energy Environ. Sci. 9 (1) (2016) 112–116.
[18] Y. Deng, C. Eames, J.-N.l. Chotard, F. Lalere, V. Seznec, S. Emge, O. Pecher, C.P. Grey, C. Masquelier, M.S. Islam, Structural and mechanistic insights into fast lithium-ion conduction in Li4SiO4–Li3PO4 solid electrolytes, J. Am. Chem. Soc. 137 (28) (2015) 9136–9145.
[19] N. Kuwata, N. Iwagami, Y. Matsuda, Y. Tanji, J. Kawamura, Thin film batteries with Li3PO4 solid electrolyte fabricated by pulsed laser deposition, ECS Transactions 16 (26) (2009) 53–60.
[20] M. Sumita, Y. Tanaka, M. Ikeda, T. Ohno, Theoretically designed Li3PO4(100)/LiFePO4 (010) coherent electrolyte/cathode interface for all solid-state Li ion secondary batteries, J. Phys. Chem. C 119 (1) (2014) 14–22.
[21] N.I. Ayu, E. Kartini, L.D. Prayogi, M. Faisal, Crystal structure analysis of Li3PO4 powder prepared by wet chemical reaction and solid-state reaction by using X-ray diffraction (XRD), Ionics 22 (7) (2016) 1051–1057.
[22] H. Park, S.R. Lee, Y. Lee, B. Cho, W. Cho, Bias sputtering and characterization of LiCoO 2 thin film cathodes for thin film microbattery, Mater. Chem. Phys. 93 (1) (2005) 70–78.
[23] M. Reddy, T.W. Jie, C.J. Jafta, K.I. Ozoemena, M.K. Mathe, A.S. Nair, S.S. Peng, M.S. Idris, G. Balakrishna, F.I. Ezema, Studies on bare and Mg-doped LiCoO 2 as a cathode material for Lithium ion Batteries, Electrochim. Acta 128 (2014) 192–197.
[24] J. Rana, R. Kloepsch, J. Li, T. Scherb, G. Schumacher, M. Winter, J. Banhart, On the structural integrity and electrochemical activity of a 0.5 Li 2 MnO 3· 0.5 LiCoO 2 cathode material for lithium-ion batteries, J. Mater. Chem. 2 (24) (2014) 9099–9110.
[25] P. Ghosh, S. Mahanty, M. Raja, R.N. Basu, H.S. Maiti, Structure and optical absorption of combustion-synthesized nanocrystalline LiCoO 2, J. Mater. Res. 22 (5) (2007) 1162–1167.
[26] D. Ensling, G. Cherkashinin, S. Schmid, S. Bhuvaneswari, A. Thissen, W. Jaegermann, Nonrigid band behavior of the electronic structure of LiCoO2 thin film during electrochemical Li deintercalation, Chem. Mater. 26 (13) (2014) 3948–3956.
[27] K. Kushida, K. Kuriyama, Narrowing of the Co-3d band related to the order–disorder phase transition in LiCoO 2, Solid State Communications 123 (8) (2002) 349–352.
[28] J. Rosolen, F. Decker, Photoelectrochemical behavior of LiCoO 2 membrane electrode, J. Electroanal. Chem. 501 (1) (2001) 253–259.
[29] J. Van Elp, J. Wieland, H. Eskes, P. Kuiper, G. Sawatzky, F. De Groot, T. Turner, Electronic structure of coo, li-doped coo, and licoo 2, Phys. Rev. B 44 (12) (1991) 6090.
[30] J. Xie, J.F. Oudenhoven, P.-P.R. Harks, D. Li, P.H. Notten, Chemical vapor deposition of lithium phosphate thin-films for 3D all-solid-state Li-ion batteries, J. Electrochem. Soc. 162 (3) (2015) A249–A254.
[31] A. Jena, N. Munichandraiah, S. Shivashankar, Metal-organic chemical vapor-deposited cobalt oxide films as negative electrodes for thin film Li-ion battery, J. Power Sources 277 (2015) 198–204.
[32] R. Tian, H. Liu, Y. Jiang, J. Chen, X. Tan, G. Liu, L. Zhang, X. Gu, Y. Guo, H. Wang, Drastically enhanced high-rate performance of carbon-coated LiFePO4 nanorods using a green chemical vapor deposition (CVD) method for lithium ion battery: a selective carbon coating process, ACS Appl. Mater. Interfaces 7 (21) (2015) 11377–11386.
[33] E. Biserni, N. Garino, A.L. Bassi, P. Bruno, C. Gerbaldi, Mesoporous silicon nanostructures by pulsed laser deposition as li-ion battery anodes, ECS Transactions 62 (1) (2014) 107–115.
[34] D. Fujimoto, N. Kuwata, Y. Matsuda, J. Kawamura, F. Kang, Fabrication of solid-state thin-film batteries using LiMnPO 4 thin films deposited by pulsed laser deposition, Thin Solid Films 579 (2015) 81–88.
[35] K. Kushida, K. Kuriyama, Sol–gel growth of LiCoO 2 films on Si substrates by a spin-coating method, J. Cryst. Growth 237 (2002) 612–615.
[36] M.-S. Park, S.-H. Hyun, S.-C. Nam, Mechanical and electrical properties of a LiCoO 2 cathode prepared by screen-printing for a lithium-ion micro-battery, Electrochim. Acta 52 (28) (2007) 7895–7902.
[37] P. Birke, W. Chu, W. Weppner, Materials for lithium thin-film batteries for application in silicon technology, Solid State Ionics 93 (1–2) (1996) 1–15.
[38] K.H. Kim, Y. Iriyama, K. Yamamoto, S. Kumazaki, T. Asaka, K. Tanabe, C.A. Fisher, T. Hirayama, R. Murugan, Z. Ogumi, Characterization of the interface between LiCoO 2 and Li 7 La 3 Zr 2 O 12 in an all-solid-state rechargeable lithium battery, J. Power Sources 196 (2) (2011) 764–767.
[39] B. Wang, J. Bates, F. Hart, B. Sales, R. Zuhr, J. Robertson, Characterization of thin-film rechargeable lithium batteries with lithium cobalt oxide cathodes, J. Electrochem. Soc. 143 (10) (1996) 3203–3213.
[40] Y.-H. Chen, C.-W. Wang, X. Zhang, A.M. Sastry, Porous cathode optimization for lithium cells: ionic and electronic conductivity, capacity, and selection of materials, J. Power Sources 195 (9) (2010) 2851–2862.